Non-linear dynamics in biological microtubules: solitons and dissipation-free energy transfer

IOP Conf. Series: Journal of Physics: Conf. Series **880** (2017) 012010 doi:10.1088/1742-6596/880/1/012010

Non-linear dynamics in biological microtubules: solitons and dissipation-free energy transfer

Nick E Mavromatos

King's College London, Department of Physics, Strand, London WC2R 2LS, UK

E-mail: Nikolaos.Mavromatos@kcl.ac.uk

Abstract. I review some recent developments concerning soliton solutions in biological microtubules and their significance in transferring energy without dissipation. I discuss various types of soliton solutions, as well as 'spikes', of the associated non-linear Lagrange equations describing the dynamics of a 'pseudo-spin non-linear σ-model' that models the dynamics of a microtubule system with dipole-dipole interactions. These results will hopefully contribute to a better understanding of the functional properties of microtubules, including the motor protein dynamics and the information transfer processes. With regards to the latter we also speculate on the use of microtubules as 'logical' gates. Our considerations are classical, but the soliton solutions may have a microscopic quantum origin, which we briefly touch upon.

1. Introduction

The rôle of solitons in biological systems as providers of efficient (mostly dissipation free) energy transport, in analogy with the frictionless electric current transfer in superconductivity theories, has a long history. Already in 1968, H. Fröhlich [1] have suggested that macroscopic quantum coherent phenomena may be responsible for dissipation-free energy and signal transfer in biological systems through coherent excitations in the microwave region of the spectrum due to nonlinear couplings of biomolecular dipoles. The frequency with which such coherent modes are 'pumped' in biological systems was conjectured to be of order of the inverse of the time interval $t_{\text{coherence Froehlich}} \sim 10^{-11} - 10^{-12}$ s , which is known as Fröhlich's coherence time.

Soon after, A.S. Davydov [2], proposed that *solitonic excitation states* may be responsible for dissipation-free energy transfer along the α-helix self-trapped amide in a fashion similar to superconductivity: there are two kinds of excitations in the α-helix: deformational oscillations in the α-helix lattice, giving rise to quantized excitations ("phonons"), and internal amide excitations. The resulting non-linear coupling between these two types of excitations is a Davydov soliton, which traps the vibrational energy of the α-helix and thus prevents its distortion (solitons are classical field theory configurations with finite energy). In a rather different approach, F. Popp [3] suggested that studies of the statistics of counts of photons in ultra-weak bioluminescence in the visible region of the spectrum point towards the existence of a coherent component linked to the living state.

In the 1990's a suggestion on the rôle of quantum effects on brain functioning, and in particular on conscious perception, has been put forward by S. Hameroff and R. Penrose [4], who concentrated on the microtubules (MT) [5] of the brain cells. In particular, they noted that one may view the tubulin protein dimer units of the MT as a quantum two-state system, in

coherent superposition. The model of [4] assumes, without proof, that sufficient environmental isolation occurs, so that the *in vivo* system of MT in the brain undergoes *self-collapse*, as a result of sufficient growth that allowed it to reach a particular threshold, namely a critical mass/energy, related to *quantum gravity* (orchestrated reduction method). This type of collapse should be distinguished from the standard *environmental decoherence* that physical quantum systems are subjected to [6]. In this way, the authors of [4] argue that decoherence times of order O(1 s), which is a typical time for conscious perception, may be achieved, thereby deducing that consciousness is associated with *quantum computations* in the mind.

Unfortunately, in my opinion, environmental decoherence, even for *in vivo* MT, cannot be ignored. Microtubules (MT) are fundamental constituents of most cells [5], not only the brain ones, and play a crucial rôle in the cell mytosis. They are cylindrically shaped cytoskeletal biopolymers. They are found in eukaryotic cells and are formed by the polymerization of heterodimers built of two globular proteins, alpha and beta tubulin. The MTs can grow up to 50 μm long (with an average length of 25 μm). Each MT is built of a set of macroscopic dipoles which generate dynamical electric fields, that prove crucial for an understanding of the functional properties of MT and their interactions.

One-spatial dimensional Solitons in ferreoelectric models of MT have been discussed from a rather phenomenological point of view in [7], and argued to provide efficient energy-transfer mechanisms. These solitons are kinks of an appropriate variable, on the main axis of the MT, which is associated with the appropriate projection of the dipole vectors of the MT. In a series of works [8, 9], we have developed a microsocpic *quantum electrodynamics cavity model* for MT, in which electromagnetic interactions between the electric dipole moments of the tubulin protein dimer units and the corresponding dipole quanta in the (thermally isolated) water interiors of the *in vivo* MT, are argued to be the dominant forces, inducing environmental entanglement and eventual decoherence [6] in at most $O(10^{-6} - 10^{-7})$ s. Such times are much shorter than the required time scale for conscious perception, but have been argued to be sufficient for *dissipation-less* energy transfer and signal transduction along moderately long MT of length sizes of order μm $= 10^{-6}$ m. As I will discuss below, the basic underlying mechanism is the formation of appropriate *solitonic* dipole states along the protein dimer walls of the MT, which are reminiscent of the quantum coherent states in the Fröhlich-Davydov approach. These dipoles states are classical, obtained after decoherence of quantum states, and correspond to solutions of the non-linear equations that describe the dynamics of the MT within certain models that take proper account of the dipole-dipole interactions. We have also speculated [9] that under sufficient environmental isolation, which however is not clear if it can be achieved in *in vivo* MT systems, these coherent states may provide the basis for an operation of the MT as quantum logic and information teleporting gates. In particular, it has been argued in [8] that sufficiently strong dipole-dipole interactions between ordered water molecules in the interior of the MT cavities and the dimers are responsible for providing thermal isolation, and thus sustainable conditions for the formation of coherent dipole solitonic states on the MT surface, which could then be responsible for dissipation-free energy and signal transfer. At any rate, our main concern in the above works was the search for, and modeling of, possible quantum effects in cell MT which may not be necessarily associated with conscious perception. In fact in this talk I will disentangle the latter from dissipation-free energy and signal transfer in biological matter, which I will restrict my attention to.

In this respect I will discuss some recent developments I was involved with in ref. [10], in which we discussed and classified interesting types of solitons in MTs, including one and two-spatial dimensional solutions, and in particular those with a helical shape, which have a chance of providing more realistic models for non-linear MT dynamics. I will not discuss the environment of ordered water molecules, however I will take into account dipole-dipole interactions between dimers on the MT surface and argue that they also can also provide the necessary non-linear

dynamics for the formation of solitonic dipole states. In this latter respect, the rôle of the ordered-water molecules via their dipole-dipole interactions with the MT dimers can be viewed as providing the necessary thermal isolation, according to the ideas of [8], so that the coherent solitonic states can be formed.

The structure of the talk is as follows: In the next section 2, I discuss the model for MT, which is based on the so-called pseudo-spin non-linear σ-model, and which includes dipole-dipole interactions that they were crucial in our microscopic approach [8, 9] in providing the necessary isolation from thermal losses. In the following section 3, I classify the various solitonic solutions arising from the non-linear dynamics of the model. I discuss one-, and two-dimensional representations of the solutions and their significance as far as energy transfer along the MTs is concerned. I also discuss 'spike configurations, and the properties of the associated electric fields produced by such configurations. In the concluding section, 4, I speculate on the rôle of physical systems of MTs with solitons as logical gates, which may be important for 'quantum computations' of biological matter, which in this way optimises signal and energy transduction, by appropriate decision taking processes that chose the most efficient path, minimising losses. We note that similar speculations have been made on mechanisms for light harvesting by marine algae [11].

2. The pseudo-spin σ-model for microtubules and the phase diagram

MTs are realized as hollow cylinders typically formed by 13 parallel protofilaments (PFs) covering the wall of MT [5, 12, 13]. Each PF represents a tubulin heterodimer with the electric dipole momentum, $\mathbf{P}$. (See Fig. 1.) Due to their interaction with the complex biological

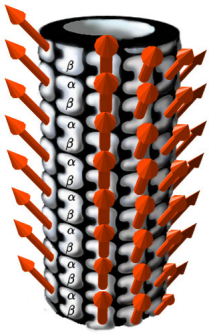

Figure 1. The structure of the cytoskeleton microtubule (MT). The arrows indicate the orientation of the permanent dipole moments of the tubulin heterodimers with respect to the MT surface. Picture from ref. [10].

environment (solvent) the MTs may experience a strong radial electrostatic field leading to the additional (radial) polarization of tubulins [14].

The tibulin heterodimer contains approximately 900 amino acid residues with the number of atoms about 14000. The total mass of the heterodimer can be estimated as, ($M \approx 1.84 \cdot 10^{-19}$g). Each heterodimer can be considered as effective electric dipole with α and β tibulin being as positive and negative side of dipole, respectively [15].

In our model [10] we treat each dipole as a classical pseudo-spin, $\mathbf{S}_i$, with a constant modulus. The potential energy of the system can be written as:

$$U_0 = \sum_{\langle i,j \rangle} J_{ij} \big(\mathbf{S}_i \cdot \mathbf{S}_j - 3(\mathbf{S}_i \cdot \mathbf{e}_{ij})(\mathbf{S}_j \cdot \mathbf{e}_{ij}) \big) - B \sum_i \mathbf{S}_i \cdot \mathbf{e}_r, \tag{1}$$

where $\mathbf{e}_{ij}$ is a unit vector parallel to the line connecting the dipoles, $\mathbf{S}_i$ and $\mathbf{S}_j$. The scalar product is understood as follows: $\mathbf{S}_i \cdot \mathbf{S}_j = S_i^1 S_j^1 + S_i^2 S_j^2 + S_i^3 S_j^3$. The first sum describes the dipole-dipole interaction, and the second one characterizes the effect of the transversal (radial) electrostatic field acting on the dipoles. The interaction coupling J_{ij} is given by $J_{ij} = \frac{1}{4\pi\epsilon\,\epsilon_0\, r_{ij}^3}$, where ϵ is the permittivity of the MT medium, ϵ_0 that of the vacuum and r_{ij} is the distance between sites i and j of the lattice model. This coupling expresses the well-known fact that dipole-dipole interactions in electromagnetism scale with the inverse of the cubic power of the distance between the dipoles.The quantity B denotes the amplitude of the effective electric field, produced by the solvent environment, along the radial direction $\mathbf{e}_r$.

Since the MTs may exhibit ferroelectric properties at room temperature, one can consider the MT as a ferroelectric system [13, 16]. To include into consideration the ferroelectric properties of the MT, we adopt the approach developed in [17]. In this case, the overall effect of the environment on the effective spin, $\mathbf{S}_i$, is described by the double-well quartic on-site potential,

$$V(\mathbf{S}_i) = P(\mathbf{S}_i \cdot \mathbf{e}_z)^2 + Q(\mathbf{S}_i \cdot \mathbf{e}_z)^4. \tag{2}$$

It is convenient to parameterize the pseudo-spin $\mathbf{S}_i$ by the unit vector $\mathbf{n}_i$, as: $\mathbf{S}_i = S\mathbf{n}_i$, where S is the module of $\mathbf{S}_i$. Then, the total potential energy of the system can be written as,

$$\begin{aligned} U = {} & S^2 \sum_{\langle i,j \rangle} J_{ij} \big(\mathbf{n}_i \cdot \mathbf{n}_j - 3(\mathbf{n}_i \cdot \mathbf{e}_{ij})(\mathbf{n}_j \cdot \mathbf{e}_{ij})\big) \\ & + \sum_i \big(PS^2(\mathbf{n}_i \cdot \mathbf{e}_z)^2 + QS^4(\mathbf{n}_i \cdot \mathbf{e}_z)^4 - BS\mathbf{n}_i \cdot \mathbf{e}_r\big). \end{aligned} \tag{3}$$

In what follows we shall use the local spherical coordinates (Θ_i, Φ_i) to define the orientation of the dipole, It is commonly accepted that coupling constants, J_{ij}, are nonzero only for the nearest-neighbor dipole moments. The system of MT dimers may be represented as a triangular lattice, as shown in Fig. 2, so that each spin has six nearest neighbors. We denote the constants of interaction between the central dipole in Fig. 2 and nearest neighbors as, $J_{0\alpha}$, and the distance between the central spin and its nearest neighbors as, d_α ($\alpha = 1, 2, \ldots, 6$), setting $d_{01} = d_{04} = a$, $d_{02} = d_{05} = b$, $d_{03} = d_{06} = c$. The corresponding angles (between the central dimer and others) are denoted as, θ_1, θ_2 and θ_3, so that: $\mathbf{e}_{01} \cdot \mathbf{e}_{01} = \cos\theta_1$, $\mathbf{e}_{01} \cdot \mathbf{e}_{02} = \cos\theta_2$, $\mathbf{e}_{01} \cdot \mathbf{e}_{06} = \cos\theta_3$.

Typical values of parameters known from the literature are: $a = 8\,\mathrm{nm}$, $b = 5.87\,\mathrm{nm}$, $c = 7.02\,\mathrm{nm}$, $\theta_1 = 0$, $\theta_2 = 58.2^\mathrm{o}$, $\theta_3 = 45.58^\mathrm{o}$, $S = 1714$ Debye [18, 17] (See Fig. 2b.) The radius of the MT can be estimated as, $R \approx 11.2\,\mathrm{nm}$ [16, 19]. The unit cell shown in Fig. 2 consists of the central spin surrounded by six neighbors. Its area is: $\Sigma_0 = 3ad = 120\,\mathrm{nm}^2$.

From now on we shall work in the Continuum approximation, which suffices for the classification of the various solutions describing the non-linear dynamics of the system. The continuum limit is obtained by allowing the area per a site, Σ_0 to go to zero, keeping the total area, $N\Sigma_0$ fixed. In this limit, the summation is replaced by the integral over the MT surface: $\sum_{\langle ij \rangle} \to (1/2)\int_\Sigma d^2x$. The variable, $\mathbf{n}_i = \mathbf{n}(\mathbf{r}_i)$, should be replaced by a smooth function of the continuum coordinates: $\mathbf{n}(\mathbf{r}_i) \to \mathbf{n}(\mathbf{r})$.

In the cylindrical coordinates the metric on Σ can be written as,

$$ds^2 = R^2 d\varphi \otimes d\varphi + dz \otimes dz, \tag{4}$$

where R is the radius of the MT. In what follows, we use the abbreviation: $\nabla n^a \cdot \nabla n^b = g^{ij}\partial_i n^a \partial_j n^b$.

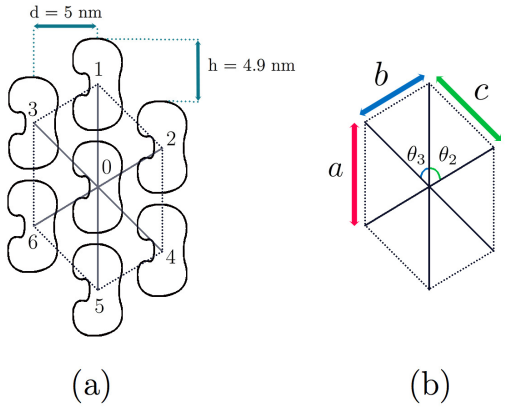

Figure 2. (Color online) Tubulin neighborhood in the hexagonal unit cell of the microtubule. The distance between dimers is d. The heterodimer helix direction is defined by the height, h. The typical values of parameters are: $a = 8\,\text{nm}$, $b = 5.87\,\text{nm}$, $c = 7.02\,\text{nm}$, $d = 5\,\text{nm}$, $h = 4.9\,\text{nm}$, $\theta_1 = 0$, $\theta_2 = 58.2^{\text{o}}$, $\theta_3 = 45.58^{\text{o}}$ [18, 16, 17, 19] .

The metric in the intrinsic space of pseudo-spins is given by: $G_{ab} = \delta_{ab} - h_{ab}$ $(a, b = 1, 2, 3)$, where

$$h_{22} = \frac{6S^2}{J}\sum_{\alpha=1}^{3} J_{0\alpha}\sin^2\theta_\alpha,\ \ h_{23} = \frac{3S^2}{J}\sum_{\alpha=1}^{3}(-1)^\alpha J_{0\alpha}\sin\theta_\alpha\cos\theta_\alpha,\ \ h_{33} = \frac{6S^2}{J}\sum_{\alpha=1}^{3} J_{0\alpha}\cos^2\theta_\alpha\ . \tag{5}$$

The computation of the constants yields: $h_{22} = 1.55$, $h_{23} = 0.11$, $h_{33} = 1.45$.

Further, it is convenient to introduce the dimensionless coordinates, $\zeta = z/\sqrt{\Sigma_0}$ and $\tilde{R} = R/\sqrt{\Sigma_0}$. Now, the total action yielding the equations of motion can be written as,

$$S_{tot} = J\int dt\int_\Sigma \mathcal{L}d\Sigma + S_\lambda, \tag{6}$$

where $d\Sigma = \tilde{R}d\zeta d\varphi$ and

$$S_\lambda = J\int dt\int_\Sigma \lambda(\mathbf{n}\cdot\mathbf{n} - 1)\,d\Sigma. \tag{7}$$

The Lagrangian of the system is given by,

$$\mathcal{L} = \frac{\rho}{2}\left(\frac{\partial\mathbf{n}}{\partial t}\right)^2 + \frac{1}{2}G_{ab}\nabla n^a\cdot\nabla n^b - \mathcal{V}(\mathbf{n}), \tag{8}$$

where $\rho = I/J$ and

$$\mathcal{V}(\mathbf{n}) = G_{ab}n^a n^b + g_0(n^3)^2 + g_1(n^3)^4 - g_2 n^1. \tag{9}$$

Taking into account that $h_{23}, |h_{33} - h_{22}| \ll 1$, we neglect by contributions of these terms and keep only terms with h_{33}. This approximation transforms the Lagrangian (8) into the following [10]

$$\mathcal{L} = \frac{\rho}{2}\left(\frac{\partial\mathbf{n}}{\partial t}\right)^2 + \frac{1}{2}(\nabla\mathbf{n})^2 - \frac{h}{2}(\nabla n^2\cdot\nabla n^2 + \nabla n^3\cdot\nabla n^3) - \mathcal{W}(\mathbf{n}), \tag{10}$$

where $h = h_{33}$ and

$$\mathcal{W}(\mathbf{n}) = h(n^1)^2 + g_0(n^3)^2 + g_1(n^3)^4 - g_2 n^1. \tag{11}$$

As one can see, in the continuum limit the electric properties of the MT are described by the nonlinear anisotropic σ-model. The order parameter, $\mathbf{n}$, is the local polarization unit vector specified by a point on the sphere, S^2.

Using the local spherical coordinates (Θ, Φ) to define the orientation of the dipole: $\mathbf{n} = (\sin\Theta\cos\Phi, \sin\Theta\sin\Phi, \cos\Theta)$, the Lagrangian of the system can be recast as follows:

$$\begin{aligned}\mathcal{L} =& \frac{\rho}{2}((\partial_t\Theta)^2 + \sin^2\Theta(\partial_t\Phi)^2) + \frac{1}{2}\big((\nabla\Theta)^2 + (\nabla\Phi)^2\big) - \frac{h}{2}(\cos\Theta\sin\Phi\nabla\Theta + \sin\Theta\cos\Phi\nabla\Phi)^2 \\ &- \frac{h}{2}\sin^2\Theta(\nabla\Theta)^2 - \mathcal{W}(\Theta,\Phi),\end{aligned} \tag{12}$$

where

$$\mathcal{W}(\Theta,\Phi) = (g_0 - h)\cos^2\Theta + g_1\cos^4\Theta - h\sin^2\Theta\sin^2\Phi - g_2\sin\Theta\cos\Phi. \tag{13}$$

The Euler-Lagrange equations can be written as [10],

$$\begin{aligned}\rho\frac{\partial^2\Theta}{\partial t^2} &= \frac{\delta\mathcal{L}}{\delta\Theta}, \\ \rho\frac{\partial}{\partial t}\left(\sin^2\Theta\frac{\partial\Phi}{\partial t}\right) &= \frac{\delta\mathcal{L}}{\delta\Phi}.\end{aligned} \tag{14}$$

The ground state of the MT, yielding the permanent dipole moment with $\Phi = 0$, is defined by the minimum value of the energy,

$$E(u) = E_0 + J\int_\Sigma \mathcal{V}(u)\, d\Sigma, \tag{15}$$

where $u = \cos\Theta$,

$$E_0 = -Jg_1\int_\Sigma \sigma^2\, d\Sigma, \tag{16}$$

and

$$\mathcal{V} = g_1\big((\sigma - u^2)^2 - \kappa\sqrt{1-u^2}\big). \tag{17}$$

Here we set $\sigma = (h - g_0)/(2g_1)$ and $\kappa = g_2/g_1$. One can see that there are three critical points: $u_1 = 0$, and $u_{2,3}$ defined from the equation:

$$u^6 - (1+2\sigma)u^4 + \sigma(2+\sigma)u^2 + \kappa^2/16 - \sigma^2 = 0. \tag{18}$$

The behavior of the dimensionless energy density of the system, $w = \mathcal{V}/g_1$, as a function of u and parameters σ and κ is presented in Fig. 3.

First, we consider the case when the parameter $\kappa = 0$. In this case, the critical points of the Hamiltonian are given by

$$u_1 = 0, \qquad u_{2,3} = \pm\sqrt{\sigma}. \tag{19}$$

As one can see, if $\sigma < 0$, the ground state of the MT is paraelectric, $u_1 = 0$. It corresponds to the radial orientation of the permanent dipole moments of the tubulin dimers with respect to the surface of the MT (Fig. 1). For $\sigma > 0$, the homogeneous ground state is a doubly degenerate ferroelectric state. The dipole momentum of the tubulin dimer is given by $u_{2,3} = \pm\sqrt{\sigma}$ (see Fig. 3a).

It follows from the phase diagram of Fig. 4 that, when $\kappa > 4\sigma$, the ground state of the MT is *paraelectric*, corresponds to the radial orientation of the permanent dipole moments of the tubulin dimers with respect to the surface of the MT. When $\kappa < 4\sigma$, the ground state of the system is *ferroelectric*.

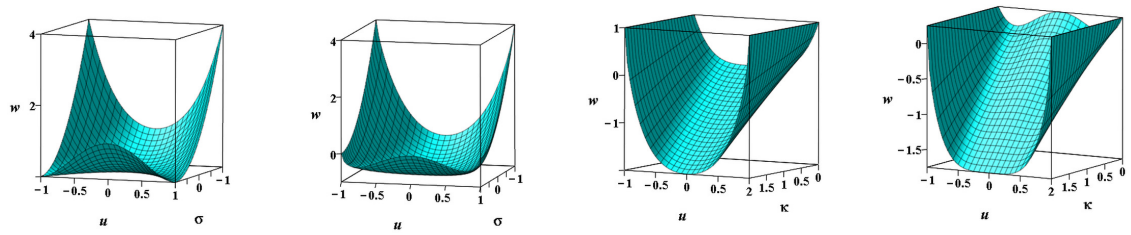

(a) (b) (c) (d)

Figure 3. Dimensionless energy density w as a function of u and parameters σ and κ. (a,b) w vs u and σ: (a) $\kappa = 0$, (b) $\kappa = 1$; (c,d) w vs u and κ: (c) $\sigma = 0$, (d) $\sigma = 0.5$.

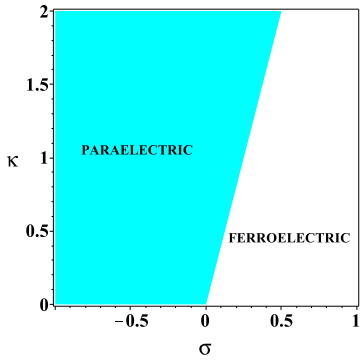

Figure 4. The phase diagram.

3. A classification of the non-linear solutions: Snoidal waves, Kinks, Helical Solitons and Spikes

In this section we proceed with a classification of the non-linear solutions of the equations of motion (14). We shall be brief in our description, referring the interested reader for details to our work in ref. [10].

In order to construct solutions for nonlinear waves moving along the MT with the constant velocity, we use the traveling wave ansatz. We assume that in cylindrical coordinates the field variables are functions of

$$\xi = \sqrt{\frac{2}{\eta p \Sigma_0}}(z + h_0\varphi/2\pi - vt), \tag{20}$$

where $\eta = h/g_1$ and $p = 1 + (h_0/2\pi R)^2$, the velocity of the wave being v. One can then show that the field equations possess the first integral of motion:

$$(u_0^2 - \cos^2\Theta)\left(\frac{d\Theta}{d\xi}\right)^2 + \sin^2\Theta\left(u_0^2 - \frac{1}{h}\cot\Theta - \sin^2\Phi\right)\left(\frac{d\Phi}{d\xi}\right)^2 + \frac{1}{2}\sin(2\Theta)\sin(2\Phi)\frac{d\Theta}{d\xi}\frac{d\Phi}{d\xi}$$
$$- (\sigma - \cos^2\Theta)^2 + \eta\sin^2\Theta\sin^2\Phi + \kappa\sin\Theta\cos\Phi = \text{const}, \tag{21}$$

where $u_0^2 = 1 - 1/h - \rho v^2/(hp\Sigma_0)$. This implies for the nonlinear wave propagation velocity v:

$$v = \sqrt{(\sigma_0^2 - u_0^2)\frac{hp\Sigma_0}{\rho}}, \tag{22}$$

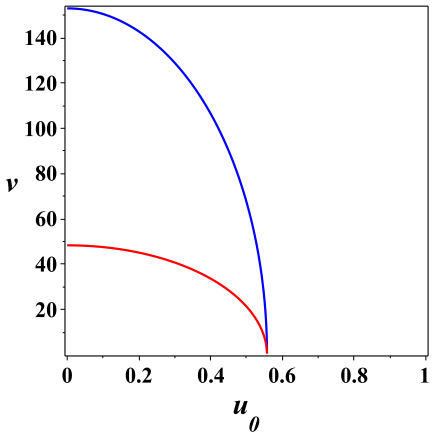

Figure 5. Velocity of the excitation (m/s): $M = 10^{-23}$ g (blue), $M = 10^{-22}$ g (red), $l = 2$ nm. From ref. [10].

where we set $\sigma_0^2 = 1 - 1/h$. The dependence of v on the parameter u_0 is depicted in Fig. 5, from which we conclude [10] that the velocity of the wave is bounded from above $v \leq v_0$, where $v_0 \approx 155$m/s.

3.1. Solutions with $\Phi = 0$

Here we discuss solutions of the system of non-linear equations (14) and (21) with $\Phi = 0$ and $\Theta = \Theta(\xi)$. For the function, $\Theta(\xi)$, we obtain the nonlinear differential equation,

$$(u_0^2 - \cos^2\Theta)\frac{d^2\Theta}{d\xi^2} + \frac{1}{2}\sin(2\Theta)\left(\frac{d\Theta}{d\xi}\right)^2 - \sin(2\Theta)(\sigma - \cos^2\Theta) + \frac{\kappa}{2}\cos\Theta = 0. \tag{23}$$

The phase portraits of the system $(\Theta(\xi), P_\Theta = d\Theta(\xi)/d\xi)$ is determined from (21), which in this case reads [10]

$$(u_0^2 - \cos^2\Theta)\left(\frac{d\Theta}{d\xi}\right)^2 - (\sigma - \cos^2\Theta)^2 + \kappa\sin\Theta = \text{const.}\ , \tag{24}$$

and are depicted in Figs. refPP1 and 7, for various parameters. One can observe the occurrence of the three elliptic points for $\sigma > u_0^2$ (Fig. 6a). When $\sigma < u_0^2$, two elliptic points disappear.

By substitution $u = \cos\Theta$ into Eq. (24), one can rewrite it as,

$$\frac{u_0^2 - u^2}{(1-u^2)}\left(\frac{du}{d\xi}\right)^2 d - (\sigma - u^2)^2 + \kappa\sqrt{1-u^2} = \text{const.} \tag{25}$$

which can be integrated to give

$$\left(\frac{du}{d\xi}\right)^2 + V(u) = 0, \tag{26}$$

where $-\varepsilon$ is the integration constant, and

$$V(u) = -\frac{((\sigma - u^2)^2 - \kappa\sqrt{1-u^2} - \varepsilon)(1-u^2)}{u_0^2 - u^2}. \tag{27}$$

Thus, the dynamics of the dipoles on the surface of the MT can be considered as the motion of the effective particle of mass $m = 2$ in the potential $V(u)$, with the total energy of the system being, $E = 0$. The phase portrait of the system (26) in the plane (Θ, P_u), with $P_u = du/d\xi$, is shown in Fig. 8.

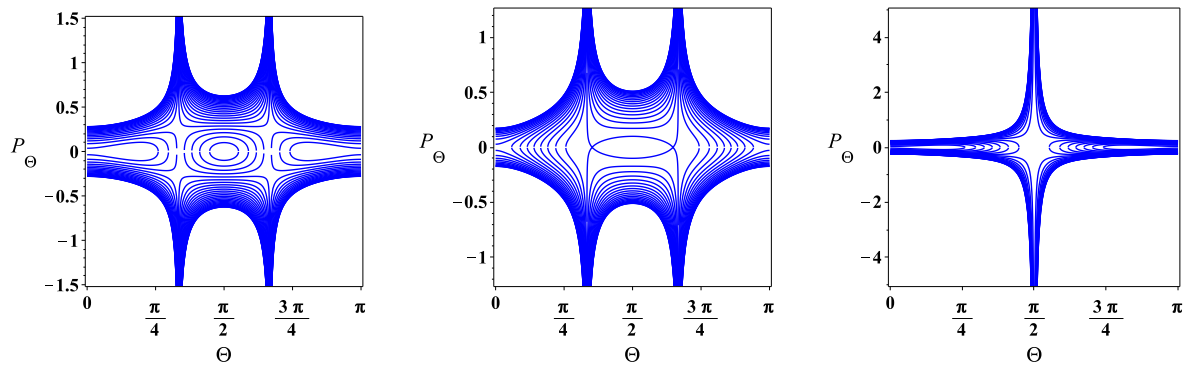

(a) (b) (c)

Figure 6. Phase portrait of the system (24). The momentum P_Θ is defined as, $P_\Theta = d\Theta/d\xi$. (a) $\sigma = 0.75$, $u_0 = 0.5$; (b) $\sigma = 0.2$, $u_0 = 0.5$; (c) $\sigma = 0.75$, $u_0 = 0$. In all cases: $\kappa = 0$. From ref. [10].

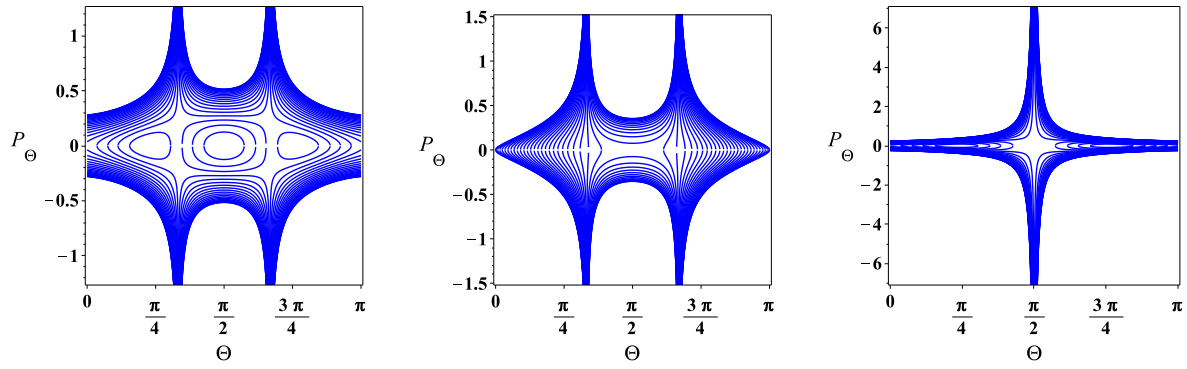

(a) (b) (c)

Figure 7. Phase portrait of the system (24). The momentum P_Θ is defined as, $P_\Theta = d\Theta/d\xi$. (a) $\sigma = 0.75$, $u_0 = 0.5$; (b) $\sigma = 0$, $u_0 = 0.5$, ; (c) $\sigma = 0.75$, $u_0 = 0$. In all cases: $\kappa = 0.5$. From ref. [10].

3.1.1. Snoidal waves and kinks: $\kappa = 0$. A sn-oidal function $\mathrm{sn}\, u$ is a particular Jacobi elliptic function. In particular, such functions are defined by means of the inverse of the following incomplete elliptic integral of the first kind [20]

$$u = \int_0^\varphi \frac{d\theta}{\sqrt{1 - m\sin^2\theta}} \Rightarrow \mathrm{sn}\, u = \sin\varphi \ , \tag{28}$$

where φ is called the amplitude, and the parameter $0 \leq m \leq 1$. Thus a sn oidal function, as all elliptic functions, are functions of two variables $(\varphi,\, m)$. [1]

To construct *sn-oidal waves* in our case, we first assume $\kappa = 0$, which implies absence of the intrinsic radial electric field ($g_2 = 0$). Choosing the constant of integration in Eq. (24) as, $\varepsilon = (\sigma - u_0^2)^2$, we obtain,

$$\left(\frac{du}{d\xi}\right)^2 = (2\sigma - u_0^2 - u^2)(1 - u^2). \tag{29}$$

[1] One can define other functions, such as $\mathrm{cn} u = \cos\varphi$ (a cn-oidal function), or $\mathrm{dn}\, u = \sqrt{1 - m\sin^2\varphi}$ (dn-oidal function).

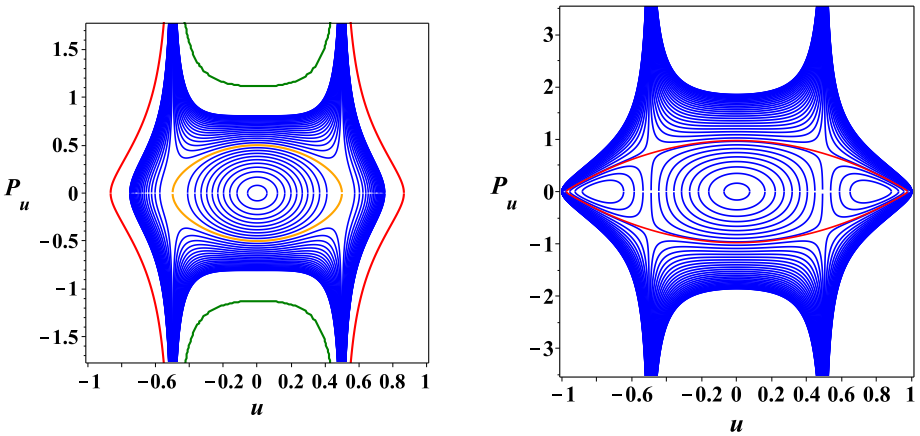

(a) (b)

Figure 8. Phase portrait of the system (25) in the plane (u, P_u): (a) $\sigma = u_0^2 = 0.25$, $k = 0.5$; (b) $\sigma = 0.6$, $k = 0.975$. Parameters: $u_0 = 0.5$, $\kappa = 0$.

Assume $u_0^2 < 2\sigma < 1 + u_0^2$, then the analytical solution of this equation is given by a snoidal wave,

$$u = k\,\mathrm{sn}(\xi - \xi_0, k). \tag{30}$$

Here $k = \sqrt{2\sigma - u_0^2}$, and $\mathrm{sn}(z, k)$ is the Jacobi elliptic function. In Fig. 9 the static sn-solutions for different choices of the constant k are depicted. In Fig. 8a, the orbit for $k = 0.5$ is represented by the orange curve.

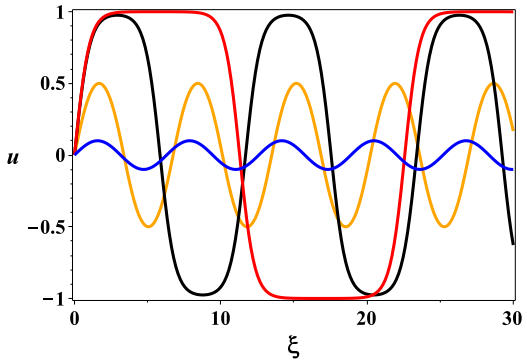

Figure 9. The sn-solution: $k = 0.1$ (blue), $k = 0.5$ (orange), $k = 0.975$ (black), $k = 0.9999$ (red).

The period of the sn-wave is given by $T = 4K$, where

$$K = \int_0^{\pi/2} \frac{d\varphi}{\sqrt{1 - k^2 \sin^2 \varphi}}, \tag{31}$$

is the complete elliptic integral of the first kind [20].

For $k^2 \ll 1$ and $k'^2 = 1 - k^2 \ll 1$, applying the Maclaurin Series in k^2 and k'^2 [20], we obtain (setting, for simplicity, $\xi_0 = 0$)

$$u = k \sin \xi - \frac{k^3}{4}(\xi - \sin \xi \cos \xi) \cos \xi + \mathcal{O}(k^5), \tag{32}$$

$$u = \tanh \xi - \frac{k'^2}{4}(\xi + \sinh \xi \cosh \xi)\mathrm{sech}^2 \xi \ . + \mathcal{O}(k'^4). \tag{33}$$

In particular, for $k = 0$, we obtain $u = 0$. This solution corresponds to the elliptic point located at the center of the phase space portrait of Fig. 8. When $k = 1$, the sn-waves become the *kink*

$$u = \tanh(\xi - \xi_0), \tag{34}$$

with the boundary conditions: $u(\pm\infty) = \pm 1$. In Fig. 8b, the corresponding orbit is presented by the separatrix (red curve).

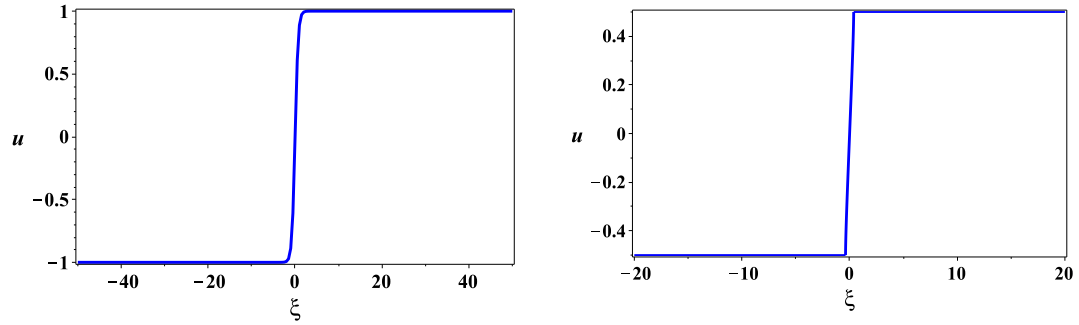

(a) (b)

Figure 10. Kink. (a) analytical solution, $\sigma = 0.25$, $\varepsilon = -0.25$. (b) numerical solution, $\sigma = 0.625$, $\varepsilon = 0.141$. Parameters: $u_0 = 0.5$, $\kappa = 0$.

A topological classification of kinks is given in terms of homotopy group [21]. The topological charge, π_0, of kink is determined by the magnitude, n_z of the polarization vector at the ends of the MT:

$$\pi_0 = \frac{1}{2}(n_z(+\infty) - n_z(-\infty)). \tag{35}$$

To change the topological charge one needs to overcome the potential barrier, proportional to the size of the MT (formally, infinite potential barrier).

We remark at this point that such one-dimensional solitions have been considered in connection with dissipation-free energy and signal transduction in phenomenological one-dimensional models of MT in [7, 8]. here such solutions have been derived from realistic three-dimensional lattice models, entailing dipole-dipole interactions, whose physical importance has been stressed above and in [8].

3.1.2. Spikes: $\kappa = 0$ A spike solution can be obtained as excitation of the ground state, u_g. To estimate energy carried by spike, we approximate it by a step function. Using Eq. (15), we then obtain [10]

$$\Delta w_{sp} = w_g - w_{sp} = -\frac{Jg_1}{\Sigma_0}(u_{sp}^2 - u_g^2)^2, \tag{36}$$

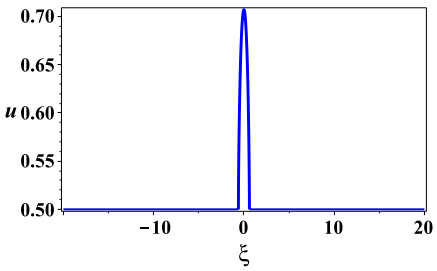

Figure 11. Spike: $\varepsilon = 0.25$, $u_0 = 0.5$, $\sigma = 0.25$, $\kappa = 0$.

where u_{sp} is the height of the spike, and $w_g = -Jg_1 u_g^4/\Sigma_0$ is the energy density of the ground state (see Eq.(16)).

The electric field produced by the spike can be estimated as [10], $\Delta E_z = E_z^{\max}(u_{sp}^2 - u_g^2)^2$, where $E_z^{\max} = \frac{Jg_1}{S}$ is the maximum value of the electric field due to the permanent dipoles, which is reached when all dipoles are aligned along the MT (in which $u_g = 1$) The maximum value of the electric field produced by spike $\Delta E_z \leq \Delta E_z^{\max}$, has been estimated in [10] as

$$\Delta E_z^{\max} = E_z^{\max}(1 - u_g^2)^2 = E_z^{\max}\cos^4\Theta_0 \leq E_z^{\max}. \tag{37}$$

where Θ_0 denotes the angle between the permanent dipole and axis orthogonal to the surface of the MT. Notice that the maximum magnitude of the electric field produced by spike is bounded by $E_z^{\max}$. As discussed in the literature [16], in the ground state the orientation of the dipoles with respect to the surface of the MT can be defined by $\Theta_0 \approx 29^{\circ}$. Substituting these data into Eq. (37), we obtain the following estimation for the electric field produced by the spike: $\Delta E_z^{\max} \approx 0.6 E_z^{\max}$. To evaluate $E_z^{\max}$, we use data available for the electric field inside of the MT: $E_z \sim 10^5 \div 10^8$ V/m [7]. Then, we obtain the following estimate for the electric field produced by the spike: $\Delta E_z^{\max} \lesssim 0.6 \cdot (10^5 \div 10^8)$ V/m . The localized spike solution is presented in Fig. 11. In the phase space portrait of Fig. 8, the corresponding orbit is indicated by the red curve on the right. We note that the spike solutions can be important candidates for information transfer by the MTs.

3.2. Solutions with $\Theta = \pi/2$ - Chiral solitons

In this section, we study solutions related to the paraelectric ground state. We seek a solution of the non-linear Lagrange equations (14) in the form: $\Theta = \pi/2$. Substituting $\Theta = \pi/2$ into Eq. (21), we obtain

$$\left(u_0^2 - \sin^2\Phi\right)\left(\frac{d\Phi}{d\xi}\right)^2 + \eta\sin^2\Phi + \kappa\cos\Phi = \text{const}, \tag{38}$$

Introducing a new function, $u_\varphi = \sin\Phi$, one can recast this equation as,

$$\left(\frac{du_\varphi}{d\xi}\right)^2 + U(u_\varphi) = 0, \tag{39}$$

where

$$U(u_\varphi) = \frac{\left(\varepsilon - \eta u_\varphi^2 - \kappa\sqrt{1-u_\varphi^2}\right)(1-u_\varphi^2)}{u_\varphi^2 - u_0^2}. \tag{40}$$

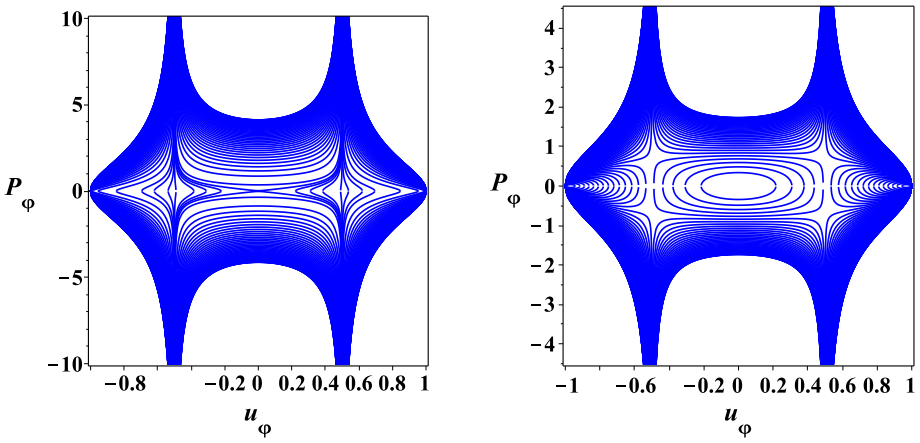

(a) (b)

Figure 12. Phase portrait of the system (39) in the plane (u_φ, P_φ): (a) $\eta = 0.1$, $\kappa = 0.75$; (b) $\eta = 0.75$, $\kappa = 0.25$. Parameters: $u_0 = 0.5$.

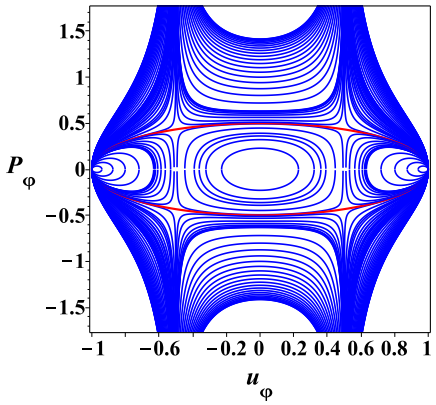

Figure 13. Phase portrait of the system (39) in the plane (u_φ, P_φ): $\eta = 0.25$, $\kappa = 0$, $u_0 = 0.5$.

We denote by ε the constant of integration in Eq. (12). "Chirality" is a topological charge described by the relative homotopy group and defined as [21]:

$$\chi = \frac{1}{\pi}\int_{-\infty}^{\infty} dz\, \mathbf{e}_z \cdot (\mathbf{n} \times \left(\left(\frac{\partial \mathbf{n}}{\partial z}\right)\right) = \frac{1}{\pi}\int_{-\infty}^{\infty} dz\, \sin^2\Theta \frac{\partial \Phi}{\partial z}. \tag{41}$$

Taking into account that in our case $\Theta = \pi/2$, we obtain $\chi = \frac{1}{\pi}(\Phi(+\infty) - \Phi(-\infty))$, Chiral solitons in the phase space are presented by orbits located in the interval $(-u_0, u_0)$. (See Figs. 12 and 13.) We remark that Chiral solitons can produce quantized charge transport across the MT that is topologically protected and controllable by the soliton's chirality.

Suppose that $\kappa = 0$, then taking the constant of integration as, $\varepsilon = \eta u_0^2$, one can rewrite (12) as:

$$\left(\frac{du_\varphi}{d\xi}\right)^2 = \eta(1 - u_\varphi^2). \tag{42}$$

The analytical solution of this equation is given by

$$u_\varphi = \sin(\sqrt{\eta}(\xi - \xi_0)) \ , \tag{43}$$

which is a *chiral soliton*. The corresponding orbit is represented in Fig. 13 by the separatrix (red curve).

3.3. Two-dimensional solutions

The solutions presented in previous sections have the form: $\Theta = \Theta(z + \nu\varphi - vt)$ and $\Phi = \Phi(z + \nu\varphi - vt)$. Thus, they describe two-dimensional nonlinear waves propagating on the MT surface along the z-direction. However, in realistic cases one may have fully two-dimensional solutions propagating on the MT surface. In Fig. 14a,b, the static helicoidal sn-solution is depicted. In Fig. 14c, the helicoidal sn-wave is presented. Finally, in Fig. 15, the solution describing kink moving in the z-direction, is depicted. All parameters are given in the corresponding figure captions. In addition one has

$$(u_0^2 - \cos^2\Theta)\Big(\frac{d\Theta}{d\xi}\Big)^2 - (\sigma - \cos^2\Theta)^2 + \kappa\sin\Theta = \text{const.} \tag{44}$$

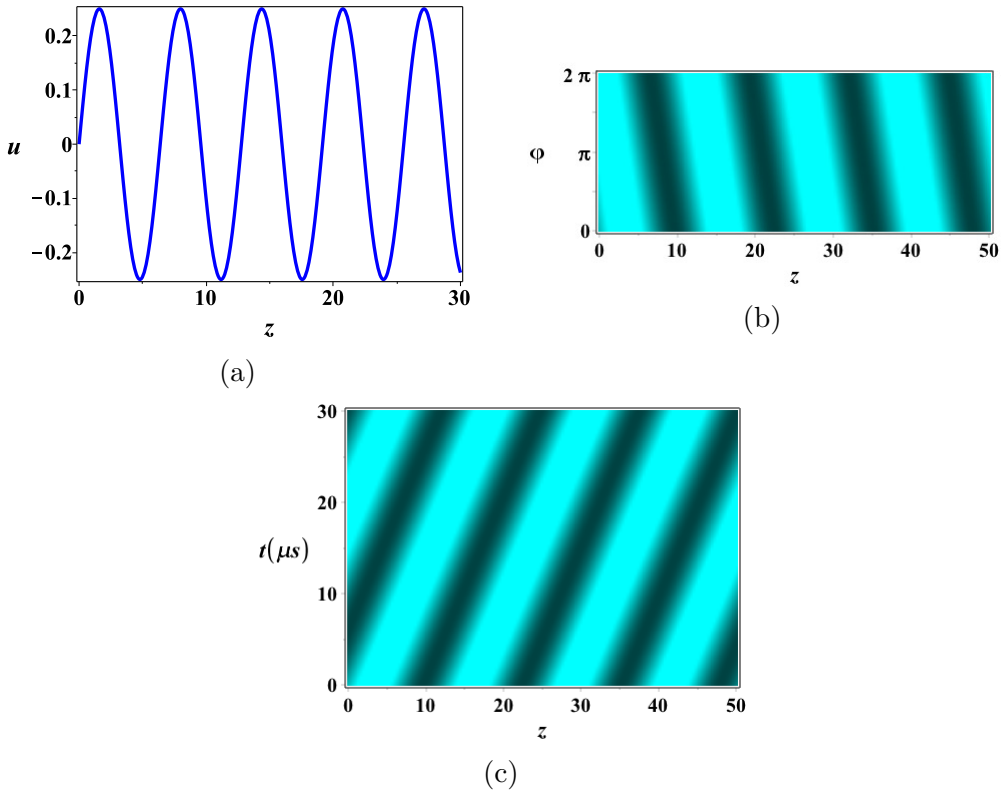

Figure 14. Sn-solutions. (a) u vs z ($v = \nu = 0$); (b) Density plot of the helicoidal static snoidal solution $v = 0$. Density plot of the propagating sn-wave along the MT ($\varphi = \text{conts}$). Parameters: $v = 0.1\text{m/s}$, $\nu = 100\,\text{nm}$, $C = 0.5$, $k = 0.25$.

This completes the classiifcation of the soliton solutions arising from the non-linear dynamics of the pseudospin model of MT.

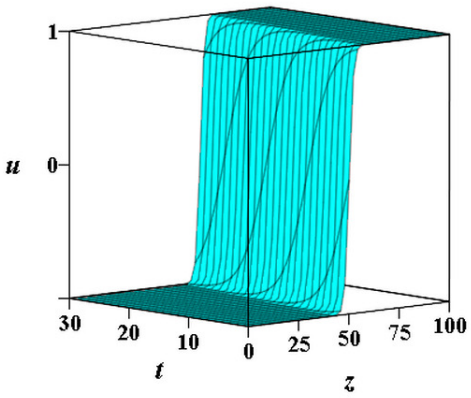

Figure 15. Propagating kink excitation. Parameters: $v = 0.1m/s$, $\nu = 100\,\mathrm{nm}$, $C = 0.5$, $k = 0.25$.

4. Conclusions and outlook

In this talk, I reviewed some recent work on soliton solutions arising in the non-linear dynamics of dimer dipoles in MicroTubular bio-systems modelled by pseudo spin non-linear σ-models. The presence of such solitons, if confirmed in realistic MT systems [22], would be an important step towards our understanding of energy and signal transduction by these biological entities. Solitons may transport energy and information in a dissipation-free and thus efficient way for the complex biological processes MT are associated with.

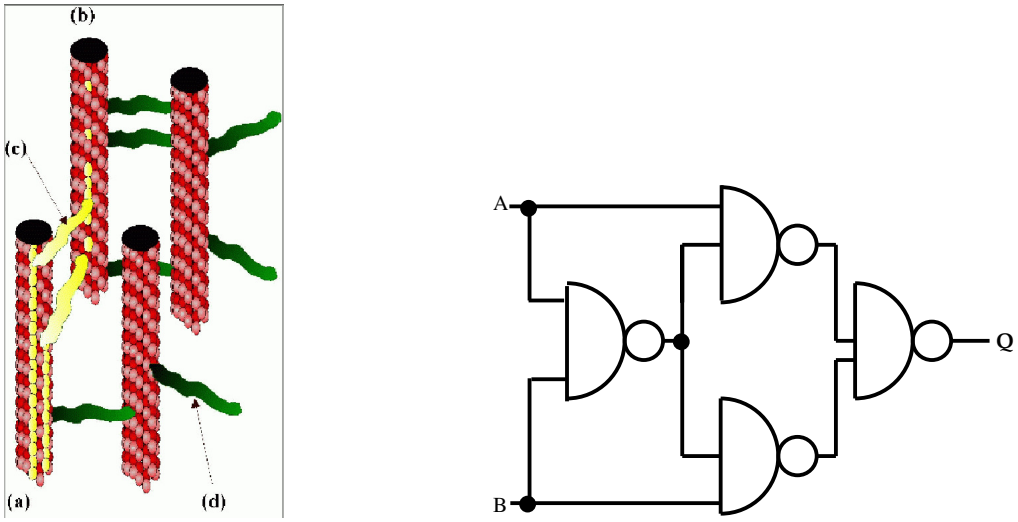

Figure 16. A MT arrangement in cell as a 'logic' XOR gate. Left panel: the biological arrangement. Right panel: the electronic XOR gate for comparison.

In addition to efficient energy transport, the presence of solitonic structures in MT, may imply their rôle as biological gates [9] (See Fig. 16, left panel). Although MT do not naturally branch, nevertheless the analogue of a 'logic' XOR gate (see Fig. 16, right panel) by MT arrangements

in cells can be provided due to the existence of Microtubule Associated Proteins (MAP) that connect the various MTs in a network. Once a soliton is formed along one MT, an "active MAP" (yellow colour in left panel of Fig. 16) can transport it from one MT to another. In the MT arrangement depicted on the left panel of Fig. 16, an XOR logic gate can be realised provided the "0" entry is represented by the absence of a soliton and the "1" entry by the presence of a soliton. In this arrangement, MT (a) acts as the "Input" MT, whilst MT (b) is the "Output" MT. (c) is a MAP transmitting a soliton, while (d) represents a "quiet" MAP (green coloured MAPs). MT (a) has two solitons travelling (yellow colour), encountering two MAPs (yelow coloured MAPs) that transmit both solitons to MT (b). In this hypothetical scenario, the solitons arrive out of phase at MT (b) and cancel each other out. The truth table for XOR reads: $0,0 \to 0; 0,1 \to 1; 1,0 \to 1, 1,1 \to 0$. and in this case is realized by MTs if the MAPs are arranged in such a way that each can transmit a soliton independently but if they both transmit, the solitons cancel out.

The above ideas are of course speculative, but it is possible that represent reality in *in vivo* situations involving MT networks. Above we have treated the solitons as classical solutions, and in fact the XOR gate rôle of MT arrangements can be due to classical physics. However, we have already mentioned above that in ref. [8] the solitons have been viewed as *macroscopic quantum coherent states*, which may survive long enough so that certain processes such as energy and signal transport along moderately long MT of length of a few μm can take place. In [8] we have discussed the conditions under which such a situation can be realised in nature, provided sufficient isolation of the MT dimer system from thermal and in general environmental losses occurs. Strong dipole-dipole interactions between the dipole moments of water molecules in the interior of the MT and the electric dipoles of the MT surface dimers have been argued to provide such conditions. In view of the logic gate representation of MT arrangements, then, it is evident that such a binary information system can provide the basic substrate for quantum information processing inside a (not exclusively neural) cell. In a typical MT network, there may be about 10^{12} tubulin dimers. Such a number is macroscopic, and one is tempted to express doubt as to whether, in realistic biological situations, such macroscopic populations of 'particles' can be entangled quantum mechanically, with the entangled state being maintained for a relatively long period of time. However, in atomic physics the experiments of ref. [23] have demonstrated *experimentally* the existence of long-lived entangled states of *macroscopic* populations of Cs gas samples, each sample containing 10^{12} atoms. In such experiments entanglement is generated via interaction with pulses of light. Thus it is not impossible that *in vivo* one has, under certain circumstances specified above, similar entanglement of MT coherent quantum states.

Acknowledgments
I would like to thank the organisers of DICE2016 for their invitation to speak in a plenary session and for organising such an interesting and thought stimulating meeting. I also acknowledge interesting discussions with my co-authors in this research and thank them for the enjoyable collaborations.

References
[1] Fröhlich H 1968 *Int. J. Quantum Chem.* **2** 641; *do.* 1970 *Nature* **228** 1093; *do.* 1972 *Phys. Lett.* **39A** (2) 153; also in *Bioelectrochemistry* eds F Guttman and H Keyzer (New York: Plenum 1986)
[2] Davydov A S 1977 *J. Theoretical Biology* **66** (2) 379
[3] Popp F A 1979 *Electromagnetic Bio- Information* eds F A Popp, G Becker, H L König and W Peschka (Munich-Vienna-Baltimore: Urban & Schwarzenberg)
[4] Hameroff S and Penrose R 1995 *J. Consciousness Studies* **2** 98; *do.*1996 *ibid.* **3** 36; *do.* Mathematics and Computers in Simulation **40** 453
[5] See, *e.g*: Dustin Y 1984 *MicroTubules* (Berlin: Springer); Engleborghs Y 1992 *Nanobiology* **1** 97
[6] Zurek W H 2003 *Rev. Mod. Phys.* **75** 715, and references therein

[7] Satarić M V, Tuszyński J A and Žakula R B1993 *Phys. Rev.* E **48** 589
[8] Mavromatos N E and Nanopoulos D V 1997 *Int. J. Mod. Phys.* B **11** 851; *do.* 1998 *ibid.* **12** 517; *do.* 1998 *Adv. Struct. Biol.* **5** 283
[9] Mavromatos N E 1999 *Bioelectrochemistry and Bioenergetics* **48** 273; Mavromatos N E, Mershin A and Nanopoulos D V 2002 *Int. J. Mod. Phys.* B **16** 3623
[10] Nesterov A I, Ramírez M F, Berman G P and Mavromatos N E 2016 *Phys. Rev.* E **93** 062412
[11] Collini E, Wong C Y, Wilk K E, Curmi P M G, Brumer P and Scholes G D 2010 *Nature* **463** 644
[12] Tuszyński J A, Brown J A, Hawrylak P and Marcer P 1998 *Phil. Trans. R. Soc. Lond. A* **356** 1897
[13] Satarić M V and Tuszynski J A 2005 *J. Bio. Phys.* **31** 487
[14] Baker N A, Sept D, Simpson J, Holst M J and McCammon J A 2001 *Proc. Nat. Acad. Sci.* **98** 10037
[15] Satarić M V 2014 *Bulletin T. CXLVI Acad. Serb. Sci. et Art.* **39** 1
[16] Tuszyński J A, Brown J A, Crawford E, Carpenter E J, Nip M L A, Dixon J M and Satarić M V 2005 *Mathematical and Computer Modelling* **41** 1055
[17] Tuszyński J A, Hameroff S, Satarić M V, Trpisova B and Nip M L A 1995 *J. Theor. Biol.* **174** 1055
[18] Slyadnikov E E 2011 *Technical Physics* **56** 1699
[19] Tuszynski J A and Craddock T J A 2010 *J. Biol. Phys.* **36** 53
[20] Abramowitz M and Stegun I A 1964 *Handbook of Mathematical Functions with Formulas, Graphs, and Mathematical Table* (Dover Publications)
[21] Mermin N D 1979 *Rev. Mod. Phys.* **51**(3) 591
[22] Sahu S, Ghosh S, Hirata K, Fujita D and Bandyopadhyay A 2013 *Appl. Phys. Lett.* **102** 123701
[23] Julsgaard B, Kozhekin A and Polzik E 2001 *Nature* **413** 400